

QCD and Rescattering in Nuclear Targets

Jianwei Qiu^a and George Sterman^b

^a *Department of Physics and Astronomy, Iowa State University
Ames, Iowa 50011*

^b *C.N. Yang Institute for Theoretical Physics, State University of New York
Stony Brook, NY 11794-3840*

Abstract

We review the extension of the factorization formalism of perturbative QCD to soft rescattering associated with hard processes in nuclei.

1 Introduction

This paper reviews a perturbative QCD (pQCD) treatment of the hard scattering of hadrons and leptons in nuclei, based on factorization. It describes in part work in collaboration with Ma Luo [1, 2, 3] and Xiaofeng Guo [4, 5, 6]. At the outset, it may be useful to clarify the relation of this work to the works of Baier *et al.* (BDMPS) [7] and Zakharov [8]. For more recent progress in relating these two approaches, see [9]. We have tried to illustrate this relation schematically in Fig. 1. The BDMPS analysis begins (Fig. 1a) with the classic treatment of radiation induced when a charged particle passes through a large target, due originally to Landau, Pomeranchuk and Migdal (LPM). This analysis does not require the presence of a hard scattering, but describes the coherent results of many soft scatterings. Its primary subject has traditionally been induced energy loss. Our analysis (GLQS) begins with the perturbative QCD treatment of hard-scattering in a relatively small target (Fig. 1b), in which the primary subject of interest is momentum transfer. A complete analysis (Fig. 1c) of hard scattering in a large target involves both energy loss and the transverse momenta due to initial- and final-state soft scatterings. Our work is a step in this direction, attempting to stay as close as possible to the pQCD formalism, in which we may readily quantify corrections. To be specific, we consider only a single soft initial- or final-state interaction in addition to the hard scattering. Our central observation is that for suitably-defined jet and related inclusive cross sections this is the first order in an expansion in the quantity

$$\frac{A^{1/3} \times \lambda^2}{Q^2}, \quad (1)$$

where λ represents a nonperturbative scale, which we shall identify with a higher-twist parton distribution below. That additional scatterings are suppressed by factors of $1/Q^2$ is perhaps surprising. Let us review why this is the case, at least for certain cross sections.

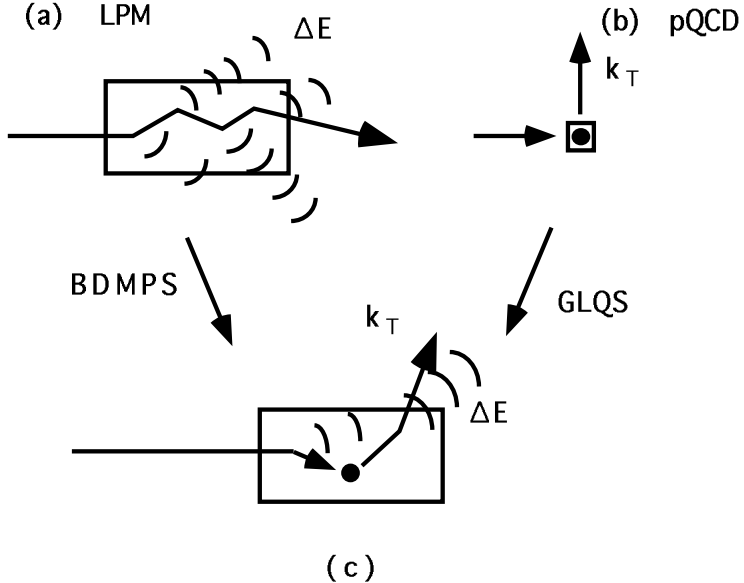


Figure 1: Alternate approaches to hard scattering in nuclei. (a) Landau-Pomeranchuk-Migdal analysis treats energy loss due to many soft scatterings. (b) Perturbative QCD analysis treats momentum transfer due to hard scattering. (c) For scattering in nuclei, both must be combined.

The basic analysis of hard-scattering in nuclear matter (cold or hot) [10] is quite simple. To be specific, consider the scattering of a quark, as shown in Fig. 2. A hard-scattering with momentum transfer Q can resolve states whose lifetimes are as short as $1/Q$, for instance quarks off-shell by order Q , but still less than Q . The off-shellness of the scattered quark increases with the momentum transfer simply because *the number of available states increases with increasing momentum*. Similarly, the scattered quark, of momentum p' is typically off-shell by order $m_J \leq Q$. We may think of m_J as the invariant mass of the jet into which quark fragments. If we are to recognize the jet, we must have $m_J \ll E_J = p'_0$, with E_J being energy of the jet. On the other hand, the counting of available states ensures that $m_J \gg \Lambda_{\text{QCD}}$.

Now the scattered quark has a lifetime in its own rest frame $\Delta t^{(p')} \sim \frac{1}{m_J}$ with $m_J \ll E_J$. In the target rest frame, however, this becomes, for large enough E_J/m_J , $\Delta t^{(\text{target})} \sim \frac{1}{m_J} \left(\frac{E_J}{m_J} \right) > R_A$, where R_A is the (fixed) target size. Thus, at high enough energy the lifetime of the scattered quark will exceed the target size, even though the quark itself is far off the mass shell, typically by a scale that grows with the momentum transfer Q .

Further couplings of the off-shell quark are suppressed, first of all by the strong coupling evaluated at scale m_J , and, more importantly, by an overall factor of $1/m_J^2 \sim 1/Q^2$, since the effective size of the scattered quark decreases with momentum transfer in this manner.

In summary, for inclusive processes such as jet production, high- Q implies that process-dependent multiple scattering is power-suppressed compared to single scattering. The most important point here is that the scattered particle remains off-shell for its entire transit of the target. Thus, its interactions with the target may be treated by the formalism of perturbative QCD, which, however, must be extended to include corrections that decrease

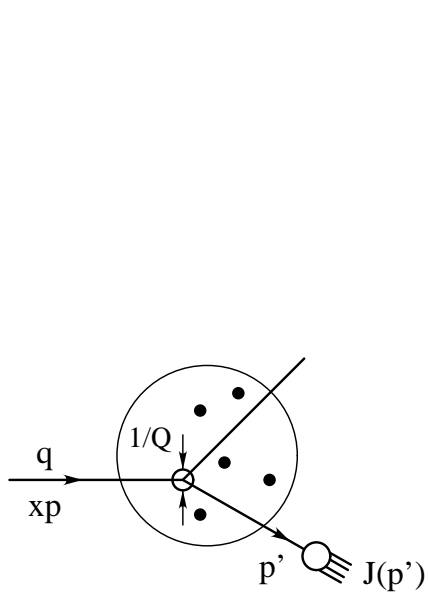


Figure 2: Sketch for the scattering of a quark of momentum xp in a large nucleus.

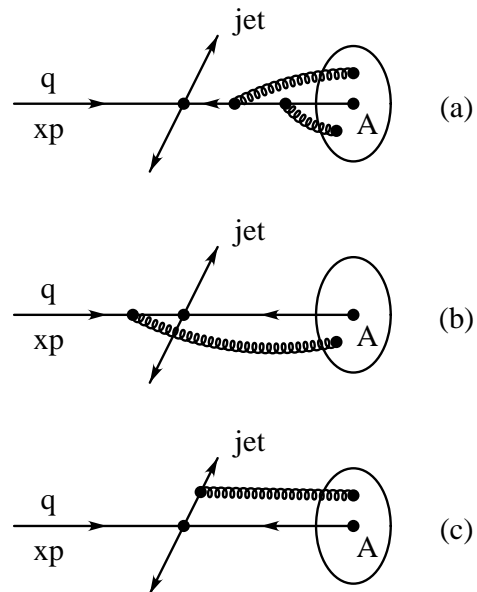


Figure 3: Classification of parton multiple scattering in nuclear medium: (a) interactions internal to the nucleus, (b) initial-state interactions, and (c) final-state interactions.

with extra powers of momentum transfer. Up to the first such “higher-twist” contribution, a general cross section has the representation [11]

$$\sigma(Q) = H^0 \otimes f_2 \otimes f_2 + \left(\frac{1}{Q^2} \right) H^1 \otimes f_2 \otimes f_4 + O \left(\frac{1}{Q^4} \right), \quad (2)$$

where \otimes represents convolutions in fractional momenta carried by partons, and f_n represents a parton distribution of twist n . Target-size dependence due to multiple scattering can only appear in the second term in this expansion.

2 Parton-Nucleus Scattering in Perturbative QCD

To distinguish parton-nucleus multiple scattering from partonic dynamics internal to the nucleus, we classify the multiple scattering internal to a nuclear target in the following three categories: (a) initial-state interactions internal to the nucleus, (b) initial-state parton-nucleus interactions (ISI), and (c) final-state parton-nucleus interactions (FSI), as shown in Fig. 3. To a certain degree, this classification is ambiguous, but it can be made well-defined if we are careful.

Initial-state interactions internal to the nucleus change the twist-2 parton distributions of the nucleus, as shown in Fig. 3a. As a result, the effective parton distributions of a large nucleus are different from a simple sum of individual nucleon’s parton distributions. This is known as the “EMC” effect for the region where the parton’s momentum fraction x is

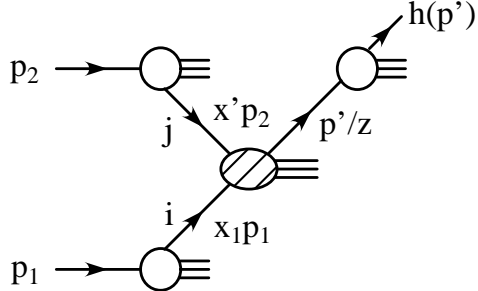


Figure 4: Scattering amplitude between two incoming hadrons with one hard collision.

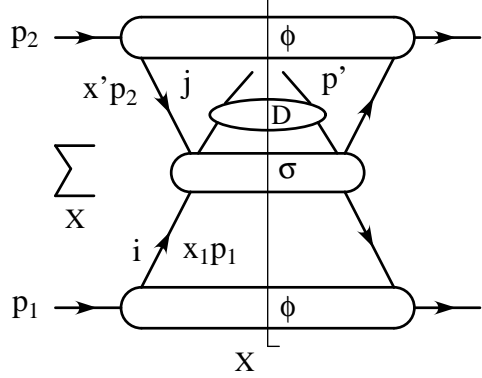


Figure 5: Perturbative QCD factorization at leading twist.

not too small. Since only a single parton from the nucleus participates the hard collision to leading power, the effect of the initial-state interactions internal to the nucleus is (almost by definition) leading twist. The A -dependence of the “EMC” effect provides a relatively small nuclear size dependence to the first term in the Eq. (2).

On the other hand, the initial-state and final-state parton-nucleus interactions, as shown in Fig. 3b and 3c, involve at least two physical partons from the nucleus at the hard collisions. Thus the “Cronin effect”, A^α -dependence with $\alpha > 1$, due to multiple scattering, is higher-twist for inclusive distributions.

2.1 Factorization at Leading Powers

Let us review some of the details of a factorized cross section like the one in Eq. (2).

The leading power contributions to a general cross section involve only one hard collision between two partons from two incoming hadrons (or nuclei), as shown in Fig. 4. An energetic third parton is produced in the collision, which fragments into either a jet or a hadron of momentum p' . After squaring the scattering amplitude in Fig. 4, and summing over all final-states, the cross section can be factorized into a form like the first term in Eq. (2),

$$\omega \frac{d\sigma_2}{d^3 p'} = \sum_{ijk} \int \frac{dx'}{x'} f_{j/p_2}(x') \int \frac{dx_1}{x_1} f_{i/p_1}(x_1) \int \frac{dz}{z^2} D_{h/k}(z) \hat{\sigma}_{ij \rightarrow k}(x_1 p_1, x' p_2, p'/z), \quad (3)$$

where \sum_{ijk} runs over all parton flavors and all scale dependence is implicit. The $D_{h/k}$ are fragmentation functions for a parton of type k to produce a hadron h . For jet production, the fragmentation from a parton to a jet, suitably defined, is calculable in perturbation theory, and may be absorbed into the “hard scattering function” $\hat{\sigma}$. Then, the factorized single scattering formula in Eq. (3) is reduced to the first term in Eq. (2). The $f_{a/p}$ are twist-2 distributions of parton type a in hadron p . They have the interpretation of expectation values in the hadronic state of products of fields on the light cone, for instance, for a quark

distribution

$$f_{q/p}(x, Q) = \int \frac{dy^-}{2\pi} e^{ixp^+y^-} \langle p | \bar{q}(0) \frac{\gamma^+}{2} q(y^-) | p \rangle, \quad (4)$$

where for simplicity we choose the $A^+ = 0$ gauge, assuming \vec{p} is in the plus direction. Eq. (3) is illustrated by Fig. 5. As shown, the convolution in Eq. (3) is in terms of the momentum fractions x_1 and x' carried by partons i and j , from hadrons p_1 and p_2 , respectively, into the hard scattering.

The factorized formula in Eq. (3) illustrates the general leading power collinear factorization theorem [12]. It consistently separates perturbatively calculable short-distance physics into $\hat{\sigma}$, and isolates long-distance effects into universal nonperturbative matrix elements (or distributions), such as $f_{a/p}$ or $D_{h/k}$, associated with each observed hadron. Quantum interference between long- and short-distance physics is power-suppressed, by the large energy exchange of the collisions. Predictions of pQCD follow when processes with different hard scatterings but the same nonperturbative matrix elements are compared.

In the case of collisions on a nuclear target, the factorized single scattering formula remains valid, except that the twist-2 parton distribution $f_{a/p}$ is defined on a nuclear state, instead of a free nucleon state. For example, for a nucleus of momentum $P_A \equiv A p_A$, the effective quark distribution is defined in the same way as in Eq. (4), with $|p\rangle$ a nuclear state, $|P_A\rangle$. Such an effective nuclear parton distribution includes the “EMC” effect, and is still a twist-2 distribution function by the definition of its operator.

Power-suppressed corrections to Eq. (3) involve ratios of the nonperturbative momentum scales in the hadron, $\lambda \sim \Lambda_{\text{QCD}} \sim 1/\text{fm}$, over the energy exchange of hard collisions, Q , as $(\lambda^2/Q^2)^n$. These corrections can come from several different sources, including the effect of partons’ non-collinear momentum components, and the effects of interactions involving more than one partons from each hadron. In the case of nuclear collisions, such power-suppressed collisions can be enhanced by the nuclear size, as in Eq. (1).

2.2 Factorization at Nonleading Powers

Much of the predictive content of pQCD is contained in factorization theorems like Eq. (3). In order to consistently treat the power suppressed multiple scattering, we need a corresponding factorization theorem for higher-twist (i.e., power suppressed) contributions to hadronic hard scattering.

Fig. 6 is a picture for a power suppressed contribution to hard scattering. In this case, two partons i and i' with momenta $x_1 p_1$ and $x_2 p_1$ from the target (the “nucleus”) collide with a single parton j of momentum $x' p_2$ (from the “projectile”). After squaring the scattering amplitude in Fig. 6, and summing over all final states, the power suppressed contribution to the cross section can be factorized into the form [11]

$$\omega \frac{d\sigma_4}{d^3 p'} = \sum_{(ii')jk} \int \frac{dx'}{x'} f_{j/p_2}(x') \int \frac{dz}{z^2} D_{h/k}(z) \quad (5)$$

$$\times \int dx_1 dx_2 dx_3 T_{(ii')/p_1}(x_1, x_2, x_3) \hat{\sigma}_{(ii')+j}^{(4)}(x_i p_1, x' p_2, p'/z), \quad (6)$$

which can be illustrated by the sketch in Fig. 7. The expectation value T corresponding to

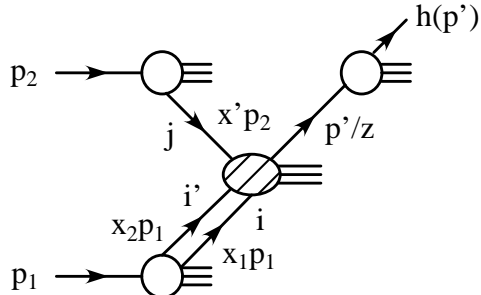


Figure 6: Scattering amplitude between two incoming hadrons with two hard collision.

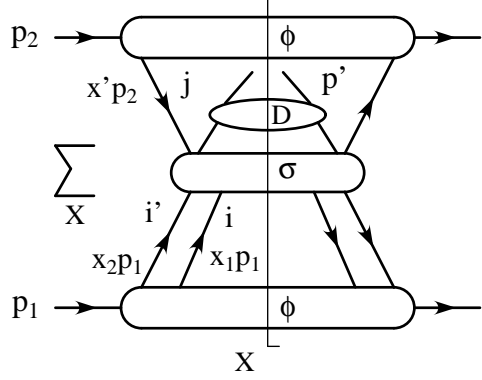


Figure 7: Perturbative QCD factorization at the next-to-leading power.

this multiparton contribution from the target is typically of the form [11],

$$T_{(ii')/p}(x_1, x_2, x_3, Q) = \int \frac{dy_1^- dy_2^- dy_3^-}{(2\pi)^3} e^{ip^+(x_1 y_1^- + x_2 y_2^- + x_3 y_3^-)} \langle p | B_i^\dagger(0) B_{i'}^\dagger(y_3^-) B_{i'}(y_2^-) B_i(y_1^-) | p \rangle, \quad (7)$$

where B_i is the field corresponding to a parton of type $i = q, \bar{q}, G$. In Eq. (6), the hard part $\hat{\sigma}_{(ii')+j}^{(4)}$ depends on the identities and momentum fractions of the incoming partons, but is otherwise independent of the structure – in particular the size – of the target (and projectile). To find A -enhancement due to multiple scattering, we must look elsewhere.

Before identifying the source of the A -enhancement, we briefly explain why the factorization formula in Eq. (6) can be valid. Although the formal arguments for the validity are well-documented [11], a heuristic understanding of factorization can be useful. Such a understanding may be found in the Lorentz transformation properties of gauge fields [13].

In hadron-hadron collisions, the factorization could be broken if interactions of long-range fields, labeled by “ S ” in Fig. 8, between the two incoming hadrons are important. The interactions of the long-range fields could alter the hadronic states of the incoming hadrons, and subsequently, change the parton matrix elements (or distributions) before the hard collisions take place. Without universality of the parton matrix elements (or distributions) in Eqs. (3) and (6), the factorized formulas would lose predictive power, and we would say that factorization is broken. Formal proofs of the factorization theorem must show that all such long-range soft interactions are either power suppressed, or can be effectively removed due to unitarity, for inclusive observables [12].

Let us now review a heuristic argument that soft interactions between the two incoming hadrons are kinematically suppressed, due to the Lorentz transformation properties of gauge fields [13]. Consider a collision between hadron A and hadron B , as shown in Fig. 9. Hadron B is moving very fast along the direction of x_3 with $\beta \sim 1$, while hadron A is at rest in the x' frame. Let us define $\Delta \equiv \beta c t' - x'_3$, where x'_3 is the third component in the x' frame. The long-range fields generated by hadron B , at rest in the x frame, behave very differently in the x and x' frames, and different types of fields have different properties under Lorentz

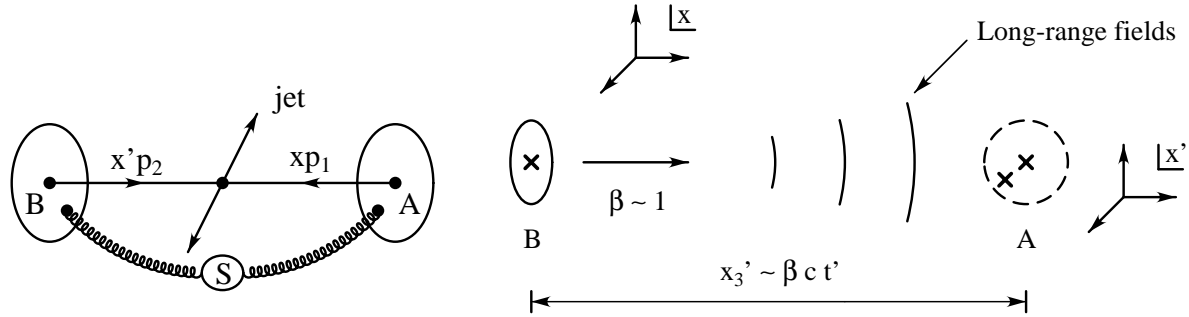


Figure 8: Interactions of long-range fields that might break the factorization.

Figure 9: Sketch for soft interactions of long-range fields between two colliding hadrons A and B .

transformations. For example, the three types of fields: scalar field, longitudinal component of a gauge field, and its E_3 field strength, have the following behaviors; with $\gamma = (1 - \beta^2)^{-1/2}$,

<u>Field</u>	<u>x-Frame</u>	<u>x'-Frame</u>
Scalar	$V(x) = \frac{e}{ \vec{x} }$	$V'(x') = \frac{e}{(x_T^2 + \gamma^2 \Delta^2)^{1/2}}$ $\implies \frac{1}{\gamma}$ “contracted like a ruler” (8)
Longitudinal Gauge	$A^-(x) = \frac{e}{ \vec{x} }$	$A'^-(x') = \frac{e\gamma(1 + \beta)}{(x_T^2 + \gamma^2 \Delta^2)^{1/2}}$ $\implies 1$ “not contracted!” (9)
Field Strength	$E_3(x) = \frac{e}{ \vec{x} ^2}$	$E_3(x') = \frac{-e\gamma\Delta}{(x_T^2 + \gamma^2 \Delta^2)^{3/2}}$ $\implies \frac{1}{\gamma^2}$ “strongly contracted!” (10)

Although the magnitude of the longitudinal component $A'^-(x')$ of the gauge field is not suppressed under the Lorentz transformation, as shown in Eq. (9), and its interactions can be very strong, a short calculation shows that as $\beta \rightarrow 1$, it becomes gauge equivalent to a vanishing gauge field. On the other hand, the gluon field strength is suppressed under the Lorentz transformation even more strongly than the scalar field, Eq. (8). In terms of energy scales, the $1/\gamma^2$ in Eq. (10) translates into a suppression factor of $1/Q^4$, which suggests that the factorization should be valid at the order of $1/Q^2$, and might fail at $O(1/Q^4)$ [11, 13, 14, 15].

Showing the factorization at the next-to-leading power is a beginning toward a unified discussion of $O(1/Q^2)$ effects in a wide class of processes. A systematic treatment of double scattering in a nuclear medium is an immediate application of the generalized factorization theorem.

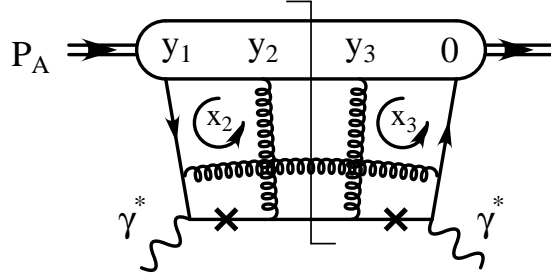


Figure 10: Poles that give rise to an A -enhanced cross section in deeply inelastic scattering.

2.3 A -Enhancement from Matrix Elements

As we pointed out in last subsection, the partonic hard part in the factorized formula in Eq. (6) is independent of the structure – in particular the size – of the target. Therefore, we need to find the A -enhancement due to multiple scattering from the matrix elements, if there is to be any size enhancement.

For definiteness, we consider photoproduction or deeply inelastic scattering on a nucleus [1, 3]. In this case, the additional soft scattering is always a final-state interaction. The structure of the target is manifest only in the matrix element T in Eq. (6). Each pair of fields in the matrix element Eq. (7) represents a parton that participates in the hard scattering. The y_i^- integrals parameterize the distance between the positions of these particles along the path of the outgoing scattered quark. In Eq. (7), integrals over the distances y_i^- generally cannot grow with the size of the target because of oscillations from the exponential factors $e^{ip^+ x_i y_i^-}$.

Since the kinematics of a single-scale hard collision is only sensitive to the total momentum from the target, two of the three momentum fractions: x_1, x_2 , and x_3 cannot be fixed by the hard collisions. If the integration of the momentum fractions is dominated by the region where $x_2 \sim 0$ and $x_3 \sim 0$, the corresponding y_i^- integration in Eq. (7),

$$\int dy_i^- e^{ix_i p^+ y_i^-} \Big|_{x_i \sim 0} \propto \text{size of the target},$$

is proportional to the size of the target or the $A^{1/3}$.

The question now is if it is possible that the partonic parts, $\hat{\sigma}_{(ii')+j}^{(4)}$ in Eq. (6) can have contributions that are dominated by regions where one or two of the three momentum fractions vanish. The answer is yes. Some of the $\hat{\sigma}_{(ii')+j}^{(4)}$ in the x_i integrals have two poles, labeled by the crosses “ \times ” in Fig. 10. The symbols “ \times ” in Fig. 10 represent the potential poles when the corresponding propagators become on-shell. In the example of deeply inelastic scattering, the poles are always associated with the scattered particle [1, 3], while in other processes, the poles can also be associated with incoming particles [4, 5]. It is important to emphasize that using a pole in the complex x_i (longitudinal momentum) space to do the integral does not correspond to assuming on-shell propagation for the scattered quark. Indeed, the x_i integrals are not pinched between coalescing singularities at such points, and the same results could be derived by performing the x_i integrals without ever going through

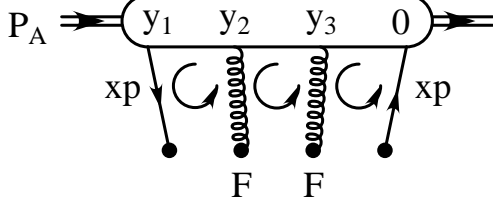


Figure 11: Sketch of the twist-4 quark-gluon correlation function that gives rise to an $A^{1/3}$ type enhancement.

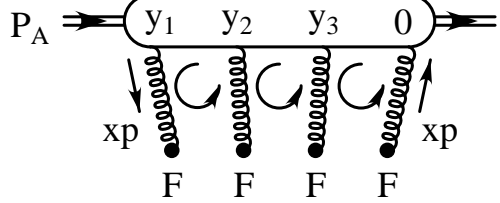


Figure 12: Sketch of the twist-4 gluon-gluon correlation function that gives rise to an $A^{1/3}$ type enhancement.

the $x_i = 0$ points. It is also worth noting that this is a feature unique to higher-twist matrix elements, for which the x_i are not restricted to be positive definite. Physically, this is possible because, unlike leading twist matrix elements, they do not generally have the interpretations of probabilities.

The result of this reasoning is that two of the three momentum fraction integrations: $dx_1 dx_2 dx_3$ in Eq. (6) are fixed by the two poles, and the convolution over $dx_1 dx_2 dx_3$ in Eq. (6) is simplified to an integration over only one momentum fraction,

$$\begin{aligned} & \int dx_1 dx_2 dx_3 T_{(ii')/p_1}(x_1, x_2, x_3) \hat{\sigma}_{(ii')+j}^{(4)}(x_i p_1, x' p_2, p'/z) \\ & \implies \int dx T_q(x, A) \hat{\sigma}_{(q)+j}^{(D)}(xp_1, x' p_2, p'/z), \end{aligned} \quad (11)$$

where the partonic part $\hat{\sigma}^{(D)}$ is finite and perturbative with the superscript (D) indicating the contribution from double scattering. The above matrix element, $T_q(x, A)$, as illustrated in Fig. 11, has the form

$$\begin{aligned} T_q(x, A) &= \int \frac{dy_1^-}{2\pi} e^{ip^+ x y_1^-} \int \frac{dy_2^- dy_3^-}{2\pi} \theta(y_2^- - y_1^-) \theta(y_3^-) \\ &\quad \times \frac{1}{2} \langle p_A | \bar{q}(0) \gamma^+ F^{\alpha+}(y_3^-) F^+_\alpha(y_2^-) q(y_1^-) | p_A \rangle, \end{aligned} \quad (12)$$

where $|p_A\rangle$ is the relevant nuclear state. The variable x here is the fractional momentum associated with the hard parton from the target that initiates the process. The soft scattering contributes a negligible longitudinal fractional momentum. Details of the reasoning and calculation for deeply inelastic scattering are given in Ref. [3].

Similar to the quark-gluon correlation function $T_q(x, A)$ in Eq. (12), another important twist-4 parton correlation function that gives rise to an $A^{1/3}$ enhancement is the gluon-gluon correlation function [1],

$$\begin{aligned} T_g(x, A) &= \int \frac{dy_1^-}{2\pi} e^{ip^+ x y_1^-} \int \frac{dy_2^- dy_3^-}{2\pi} \theta(y_2^- - y_1^-) \theta(y_3^-) \\ &\quad \times \frac{1}{xp^+} \langle p_A | F^{\beta+}(0) F^{\alpha+}(y_3^-) F^+_\alpha(y_2^-) F^+_\beta(y_1^-) | p_A \rangle, \end{aligned} \quad (13)$$

which is illustrated in Fig. 12.

In this form of the twist-4 parton-parton correlation functions, two integrals over the y^- and y_2^- can grow with the nuclear radius as fast as $A^{1/3}$. However, if we require local color confinement, the difference between the light-cone coordinates of the two field strengths should be limited to the nucleon size. Therefore, only one of the two y_i^- integrals can be extended to the size of nuclear target. The twist-4 parton-parton correlation functions are then proportional to the size of the target, that is, enhanced by $A^{1/3}$.

3 Applications

In Refs. [1] and [3], we have applied the formalism sketched above to single-particle inclusive and single-jet production for deeply inelastic scattering and photoproduction. These cases involve final-state interactions only. In each case, the leading $1/Q^2$ correction is proportional to the matrix elements in Eqs. (12) and (13). Of course, the value of the correction cannot be estimated without an idea of the magnitudes of the T 's. Since these magnitudes are nonperturbative they must be taken from experiment. At the same time, we expect the x -dependence of the probability to detect the hard parton to be essentially unaffected by the presence or absence of an additional soft scattering. Thus, we choose the ansatz [1]

$$T_i(x, A) = \lambda^2 A^{1/3} f_{i/A}(x, A) \quad (14)$$

for $i = q, g$ in terms of the corresponding twist-two effective nuclear parton distribution $f_{i/A}$, with λ a constant with dimensions of mass (see Eq. (1)). This assumption facilitates the comparison to data.

3.1 Momentum Imbalance of Di-Jets in Photoproduction

A quantity that is sensitive to final-state rescattering in a particularly direct way is the momentum imbalance of di-jets in photoproduction in nuclei. The $A^{4/3}$ dependence of this quantity measured by the Fermilab E683 collaboration is a clear signal of the presence of double scattering [16].

The di-jet momentum imbalance $k_{T\phi}$ measured at Fermilab is defined as [16]

$$k_{T\phi} \equiv \frac{1}{2} (p_{T_1} + p_{T_2}) \sin \Delta\phi, \quad (15)$$

where p_{T_1} and p_{T_2} are the transverse momenta of the di-jets and the angle between the di-jets $\Delta\phi$ is defined in Fig. 13. This momentum imbalance is the projection of the momentum imbalance out of the scattering plane defined by the beam axes and either of the two observed jets. The data from E683 shows that the averaged momentum imbalance $\langle k_{T\phi}^2 \rangle$ can be parameterized as $(1.44 + 0.174 A^{1/3}) \text{ GeV}^2$. The term proportional to $A^{1/3}$ should be a consequence of the multiple scattering of these two jets when they pass through the nuclear medium [2].

In Ref. [2], we calculated the di-jet momentum imbalance in pQCD by applying the twist-4 factorization formalism to double scattering in a nuclear medium. The lowest-order contributions to the momentum imbalance are shown schematically in Fig. 14. At the lowest

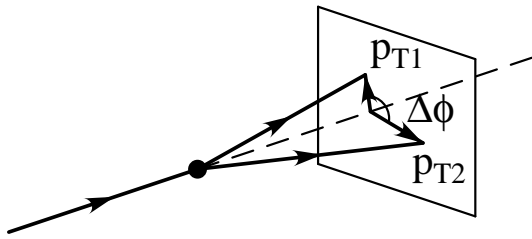


Figure 13: Sketch for the di-jet momentum imbalance measured at Fermilab E683.

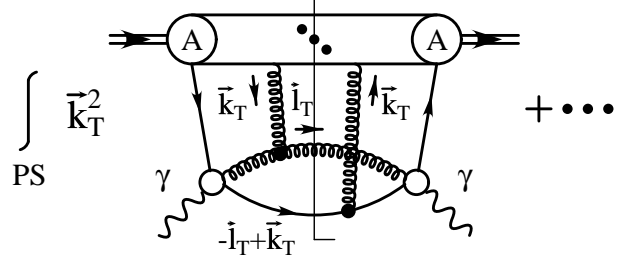


Figure 14: Sketch for the lowest order contributions to the averaged di-jet momentum imbalance in photoproduction.

order, the di-jet momentum imbalance is approximately equal to the momentum imbalance between the two scattered partons which fragment into the two leading jets: $k_T^2 \approx \hat{k}_T^2$. As shown in Figs. 13 and 14, the averaged momentum imbalance $\langle k_T^2 \rangle$ is not exactly the same as the $\langle k_{T\phi}^2 \rangle$ used in the experiment. The relation, assuming rotational symmetry, is simply (we always use rms averages)

$$\langle k_T^2 \rangle = 2 \langle k_{T\phi}^2 \rangle. \quad (16)$$

Letting $d\hat{\sigma}^{\gamma i}(xp, \ell, p_\gamma)$ denote the photon-parton Born cross section with parton flavor ($i = q, \bar{q}, g$) for fixed leading jet momentum ℓ , we derived the double scattering contribution to the momentum imbalance [2],

$$\begin{aligned} \langle k_T^2 E_\ell \frac{d\sigma^{\gamma A}(\ell)}{d^3 \ell} \rangle_{4/3} &= \lambda^2 A^{4/3} \pi^2 \alpha_s \left[C_F \sum_{i=q,\bar{q}} \int dx f_{i/A}(x) E_\ell \frac{d\hat{\sigma}^{\gamma i}}{d^3 \ell}(xp, \ell, p_\gamma) \right. \\ &\quad \left. + C_G \int dx f_{g/A}(x) E_\ell \frac{d\hat{\sigma}^{\gamma g}}{d^3 \ell}(xp, \ell, p_\gamma) \right] \end{aligned} \quad (17)$$

with $C_F = 4/3$ and $C_G = 3$. The average value of k_T^2 for all events in a region R of dijet phase space is found from Eq. (17) by integrating over that region and dividing by the corresponding un-weighted cross section [2]. If we assume that $\alpha_s(\ell_T^2)$ in Eq. (17) is evaluated at a typical value of the momentum transfer in R , and is kept approximately constant within R , the averaged momentum imbalance at the lowest order can be expressed as

$$\langle k_T^2(R) \rangle_{4/3} = \lambda^2 A^{4/3} \pi^2 \alpha_s \frac{C_F \sigma_q^{\gamma A}(R, p_\gamma) + C_G \sigma_g^{\gamma A}(R, p_\gamma)}{\sigma_q^{\gamma A}(R, p_\gamma) + \sigma_g^{\gamma A}(R, p_\gamma)}. \quad (18)$$

In this expression, the un-weighted cross sections are defined as

$$\sigma_i^{\gamma A}(R, p_\gamma) = \int_R \frac{d^3 \ell}{E_\ell (2\pi)^3} \int dx f_{i/A}(x) E_\ell \frac{d\hat{\sigma}^{\gamma i}}{d^3 \ell}(xp, \ell, p_\gamma). \quad (19)$$

By comparing Eq. (18) to data [16], we found $\lambda^2 \sim 0.05 - 0.1$ GeV 2 [2]. This value may be used to predict anomalous A -enhancement for other processes.

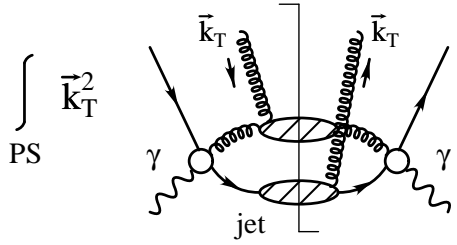


Figure 15: Sketch for the high order contributions to di-jets momentum imbalance in photoproduction.

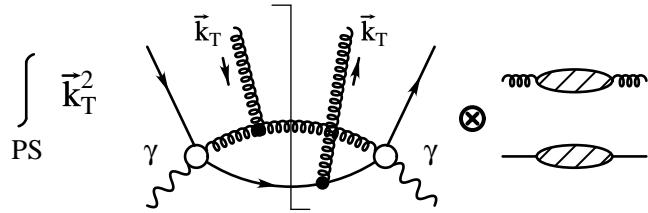


Figure 16: Sketch for the factorization of high order parton evolutions to jets from the lowest order parton level double scattering.

The lowest-order calculation given above neglects the evolution of the final state partons into jets. We have argued above, however, that the evolution of the jet takes place outside of the nucleus. It is interesting to see how this decoupling of jet evolution occurs in our calculation.

In perturbation theory, higher-order corrections due to the evolution of the final state partons in Fig. 14 arise from diagrams of the kind shown in Fig. 15. The shaded subdiagrams may be thought of as “jet functions”, which represents the evolution of the outgoing partons. The first thing to note is that leading corrections due to final-state partonic bremmstrahlung are from small angle emission, which stays within the respective jets. Such collinear emission does not change the imbalance, k_T , although any of these fragmentation products can, in principle, exchange soft gluons with the nucleus. As pointed out in Ref. [2], however, soft gluon multiple scattering cannot resolve the details of the jets. The coupling of the final-state jet to soft gluons is coherent, and equivalent to a single “eikonal” line at leading power, whose direction and color are defined by the parton that initiates the jet. Thus, soft nuclear rescatterings factor from the jets, as shown in Fig. 16. The combination of two such eikonal couplings, weighted by k_T^2 is enough to generate a lowest-order contribution to the matrix elements of Eqs. (12) or (13). At yet higher orders, but remaining at first nonleading power in Q , additional soft gluon corrections generate nonabelian phases [12], (ordered exponentials of the gauge field), which serve to make the higher-twist matrix elements gauge-invariant, but do not otherwise affect A -dependence. One way of looking at this is that the di-jet k_T imbalance is relatively insensitive to energy loss. Thus, the leading dependence of Eq. (1) is stable all orders in perturbation theory.

3.2 A -Enhancement in Other Processes

In order to test the theory, we need to identify other physical observables that are sensitive to the same twist-4 parton-parton correlation functions $T_i(x, A)$ with $i = q, g$. One such process is direct photon production at measured transverse momentum, whose very moderate A -dependence has been measured by the E706 experiment at Fermilab. In Ref. [4], it was found that the value of λ^2 above, which produces a relatively large enhancement in dijet momentum imbalance, due to final-state interactions, produces a quite small A -enhancement in photoproduction, due to initial-state interactions, consistent with experiment. This may

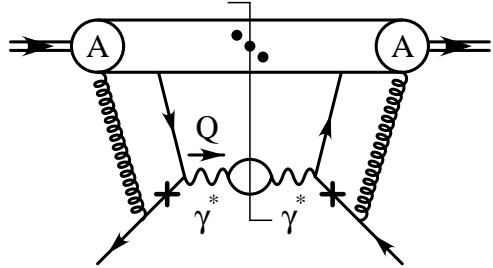


Figure 17: Lowest order diagram that contributes to the Drell-Yan transverse momentum broadening in hadron-nucleus collisions.

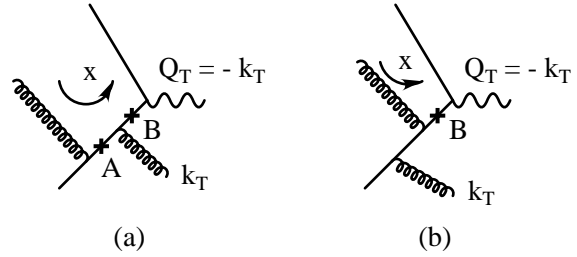


Figure 18: Sample double scattering amplitudes that contribute to the NLO A -enhancement.

shed some light on the long-standing observation that (initial-state) transverse momentum effects in Drell-Yan cross sections, to which we now turn, are also surprisingly small [17, 18, 19].

In Ref. [5], Drell-Yan transverse momentum broadening was calculated at the lowest order in pQCD. By evaluating the lowest order diagram in Fig. 17 plus corresponding interference diagrams, it was found that the Drell-Yan transverse momentum broadening in hadron-nucleus collisions can be expressed in terms of the same twist-4 quark-gluon correlation function $T_q(x, A)$ [5],

$$\langle Q_T^2 \rangle_{4/3} = \left(\frac{4\pi^2 \alpha_s}{3} \right) \frac{\sum_q e_q^2 \int dx' f_{\bar{q}/h}(x') T_q(\tau/x', A)/x'}{\sum_q e_q^2 \int dx' f_{\bar{q}/h}(x') f_q(\tau/x', A)/x'} \quad (20)$$

where \sum_q runs over all quark and antiquark flavors, e_q is the quark fractional charge, and $\tau = Q^2/s$, in terms of the lepton-pair invariant mass Q and hadron-hadron center of mass energy, \sqrt{s} . Adopting the model in Eq. (14), the lowest order Drell-Yan transverse momentum broadening in Eq. (20) can be simplified as

$$\langle Q_T^2 \rangle_{4/3} = \left(\frac{4\pi^2 \alpha_s}{3} \right) \lambda^2 A^{1/3}. \quad (21)$$

By comparing Eq. (21) to data from Fermilab E772 and CERN NA10 experiments [18, 19], it was found [5] that Drell-Yan data favor a λ value: $\lambda_{\text{DY}}^2 \sim 0.01 \text{ GeV}^2$, which is considerably smaller than the λ^2 extracted from the dijet momentum imbalance in photoproduction.

It could be that the source of this discrepancy is experimental. On the other hand, we should also consider possible differences between the roles of multiple scattering in dijet momentum imbalance and Drell-Yan. For dijet momentum imbalance in photoproduction, soft gluon multiple scatterings are purely final-state interactions, while the Drell-Yan transverse momentum broadening at the lowest order are caused by purely initial-state interactions. For initial-state interactions, there is strong interference beyond the leading order. Consider the diagrams in Fig. 18, which contribute to the Drell-Yan transverse momentum broadening,

$$\langle Q_T^2 \rangle_A = A \langle Q_T^2 \rangle_{A=1} + \langle Q_T^2 \rangle_{4/3} \quad (22)$$

at the next-to-leading order. Actually, these two diagrams can contribute to both terms in Eq. (22). In order to extract the nuclear size-enhanced contribution to the broadening (the $A^{4/3}$ term), we study the behavior of these diagrams at the poles near $x = 0$. For the diagram in Fig. 18a, there are two potential poles labeled by A and B . When k_T is small, contributions from these two poles cancel. That is, the NLO contributions to the Drell-Yan transverse momentum spectrum from this diagram do not have the dominant $1/Q_T^2$ behavior, and therefore, its contributions to the $\langle Q_T^2 \rangle_{4/3}$ is much suppressed. When k_T is small, the diagram in Fig. 18b is already included in the lowest order contribution to the broadening, because the gluon radiation is a part of the parton distribution $f_{\bar{q}/h}$. On the other hand, when k_T is large, the only possible pole at B requires a finite value of x , which ruins the A -enhancement [5].

From the above example, it seems plausible to us that the interference of initial-state radiation and multiple scattering suppresses A -enhancement in Drell-Yan cross sections. By contrast, the corresponding effects of final-state radiation may cancel for an inclusive jet cross section, because we do not observe the k_T of radiation within the high- p_T jets. For Drell-Yan, the two terms of Eq. (22) are both from initial-state interactions, while in the dijet case, the first is primarily from the initial state, while the second is final-state. In the Drell-Yan case, destructive interference between the two mechanisms is possible, for di-jets, it is not. On this basis, we may expect a stronger A -enhancement to the dijet momentum imbalance in photoproduction than to the transverse momentum in Drell-Yan. Clearly, further study of this difference between initial-state and final-state interactions and related questions is in order.

4 Conclusions

In conclusion, we have argued that the nuclear size (or $A^{1/3}$ -type) enhancement caused by multiple scattering can be consistently calculated in pQCD, in terms of generalized factorization theorems. By studying enhancement from the nuclear medium, we can learn about strong interaction physics at twist-4. The first power correction measures *new* matrix elements $\langle q(FF)q \rangle$ and $\langle F(FF)F \rangle$. These matrix elements provide new insights into the nonperturbative regime of QCD.

As reviewed above, the initial applications of pQCD to the first power corrections are interesting and generally successful. Different observables, such as jet broadening in deeply inelastic scattering [5] and pion transverse momentum broadening in deeply inelastic scattering [6], have been proposed and evaluated. The same techniques have been recently applied to many new physical observables [9, 20, 21, 22, 23, 24, 25, 26].

Acknowledgments

The work of G.S. was supported in part by the National Science Foundation, grants PHY9722101 and PHY0098527. The research of J.Q. at Iowa State was supported in part by the US Department of Energy under Grant No. DE-FG02-87ER40371.

References

- [1] M. Luo, J. Qiu and G. Sterman, Phys. Lett. B279 (1992) 377.
- [2] M. Luo, J. Qiu and G. Sterman, Phys. Rev. D49 (1994) 4493.
- [3] M. Luo, J. Qiu and G. Sterman, Phys. Rev. D50 (1994) 1951.
- [4] X. Guo and J. Qiu, Phys. Rev. D53 (1996) 6144.
- [5] X. Guo, Phys. Rev. D58 (1998) 114033. [hep-ph/9804234].
- [6] X. Guo and J. Qiu, Phys. Rev. D61 (2000) 096003.
- [7] R. Baier, Yu.L. Dokshitzer, A.H. Mueller, S. Peigné and D. Schiff, Nucl. Phys. B483 (1997) 291; Nucl. Phys. B484 (1997) 265.
- [8] B.G. Zakharov, JETP Lett. 70 (1999) 176; R. Baier, D. Schiff, and B.G. Zakharov, Ann. Rev. Nucl. Part. Sci. 50 (2000) 37.
- [9] X. Guo, X.-N. Wang, Phys. Rev. Lett. 85 (2000) 3591; Nucl. Phys. A (in press) [hep-ph/0102230].
- [10] A.H. Mueller, in *Proceedings of the XVII Rencontre de Moriond, Vol. 1*, ed. J. Tran Thanh Van, (Editions Frontieres, Gif-sur-Yvette, France, 1982).
- [11] J. Qiu and G. Sterman, Nucl. Phys. B353 (1991) 105, 137.
- [12] J.C. Collins, D.E. Soper, and G. Sterman, in *Perturbative Quantum Chromodynamics*, ed. A.H. Mueller (World Scientific, Singapore, 1989).
- [13] R. Basu, A.J. Ramalho, and G. Sterman, Nucl. Phys. B244, 221 (1984).
- [14] R. Doria, J. Frenkel, and J.C. Taylor, Nucl. Phys. B168 (1980) 93; C. Di'Lieto, S. Gendron, I.G. Halliday, and C.T. Sachrajda, Nucl. Phys. B183 (1981) 223.
- [15] F.T. Brandt, J. Frenkel, and J.C. Taylor, Nucl. Phys. B312 (1989) 589.
- [16] D. Naples *et al.* (E683 Collaboration) Phys. Rev. Lett. 72 (1994) 2341.
- [17] M.L. Swartz *et al.* Phys. Rev. Lett. 53 (1984) 32.
- [18] D.M. Alde *et al.* Phys. Rev. Lett. 66 (1991) 2285.
- [19] P. Bordalo *et al.* Phys. Lett. B193 (1987) 373.
- [20] X. Guo, Phys. Rev. D58 (1998) 036001.
- [21] R. J. Fries, B. Muller, A. Schafer and E. Stein, Phys. Rev. Lett. 83 (1999) 4261. [hep-ph/9907567].
- [22] H. Huang, Nucl. Phys. B541 (1999) 267. [hep-ph/9811292].

- [23] R. J. Fries, A. Schafer, E. Stein and B. Muller, Nucl. Phys. B582 (2000) 537. [hep-ph/0002074].
- [24] X. Guo, J. Qiu, and X. Zhang, Phys. Rev. Lett. 84 (2000) 5049; Phys. Rev. D62 (2000) 054008.
- [25] X. Guo, X. Zhang, W. Zhu, Phys. Lett. B476 (2000) 316.
- [26] H. Shen and M. Luo, Phys. Lett. B494 (2000) 63.